Staggered magnetization in $La_{2-x}Sr_xCuO_4$ from ^{139}La NQR and μSR: Effects of Sr doping in the range $0<x<0.02$

F. Borsa
Dipartimento di Fisica Generale "A. Volta," Università di Pavia, 27100 Pavia, Italy
and Ames Laboratory and Department of Physics and Astronomy, Iowa State University, Ames, Iowa 50011

P. Carretta
Dipartimento di Fisica Generale "A. Volta," Università di Pavia, 27100 Pavia, Italy

J. H. Cho,* F. C. Chou,† Q. Hu, and D. C. Johnston
Ames Laboratory and Department of Physics and Astronomy, Iowa State University, Ames, Iowa 50011

A. Lascialfari
Dipartimento di Fisica Generale "A. Volta," Università di Pavia, 27100 Pavia, Italy

D. R. Torgeson
Ames Laboratory and Department of Physics and Astronomy, Iowa State University, Ames, Iowa 50011

R. J. Gooding, N. M. Salem, and K. J. E. Vos
Department of Physics, Queen's University, Kingston, Ontario, Canada K7L 3N6
(Received 6 March 1995; revised manuscript received 9 June 1995)

We have used ^{139}La nuclear quadrupole resonance (NQR) and positive muon spin rotation (μSR) measurements to probe the weakly doped antiferromagnetic (AF) region ($x<0.02$) of the $La_{2-x}Sr_xCuO_4$ system below the three-dimensional (3D) AF ordering (Néel) temperature $T_N(x)$. From these measurements, our previous ^{139}La NQR measurements [F. C. Chou *et al.*, Phys. Rev. Lett. **71**, 2323, (1993)], and auxiliary ^{139}La nuclear magnetic resonance (NMR) measurements of single-crystal La_2CuO_4, we have determined the Cu^{2+} staggered magnetization $M^{\dagger}(x,T)$ below $T_N(x)$. Above ~ 30 K, $M^{\dagger}(x,T)$ at each T is found to be progressively depressed with increasing x (decreasing T_N); the $M^{\dagger}(x,0)$ at $T=0$, extrapolated from $T>30$ K, is found from both the NQR and μSR measurements to follow the same empirical relation $M^{\dagger}(x,0)/M^{\dagger}(0,0)=(1-x/x_c)^n$ with $x_c=0.023$ and $n=0.236$. To model the extrapolated values, we assume that the doped holes are mobile and are situated in 1D "rivers" of charge which form walls in the CuO_2 planes and which separate and uncouple undoped AF domains; an infinite number of these layers are stacked along the c axis. Using linear spin-wave theory and the interplanar and intraplanar Cu^{2+} AF exchange interactions found from neutron-scattering measurements on La_2CuO_4, we calculated $M^{\dagger}(x,0)$ for this doped hole and Cu^{2+} spin configuration and find good agreement with the above extrapolated $T=0$ values. Thus, in the AF region $x<0.02$ of the phase diagram of $La_{2-x}Sr_xCuO_4$, these results support the previous hypothesis that microsegregation of the (mobile) doped holes into domain walls occurs above ~ 30 K, consistent with the phase separation phenomenology of Emery and Kivelson. Below ~ 30 K, an anomalous increase in $M^{\dagger}(x,T)$ is observed in $La_{2-x}Sr_xCuO_4$, particularly for the larger x values approaching $x=0.02$, such that $M^{\dagger}(x,T)$ is nearly independent of x as $T\rightarrow 0$ and is therefore about the same as the $T\rightarrow 0$ value observed for undoped La_2CuO_4. We interpret this effect as arising from localization of the doped holes below ~ 30 K, whereby localized doped holes are much less effective in reducing $M^{\dagger}$ than mobile holes. In support of this hypothesis, we find that the width of the ^{139}La NQR $2\nu_Q$ line in $La_{2-x}Sr_xCuO_4$ is nearly independent of temperature below 4.2 K and increases linearly with x for $x<0.02$. We present new μSR measurements to support the idea that the effective spin degrees of freedom associated with the localized doped holes undergo a continuous freezing at $T_f\approx(815\text{ K})x$, as opposed to a cooperative phase transition, superimposed on the preexisting AF long-range order.

I. INTRODUCTION

The magnetic phase diagram of $La_{2-x}Sr_xCuO_4$ in the low doping regime, $x<0.05$, was recently constructed on the basis of static magnetic susceptibility χ and ^{139}La nuclear quadrupole resonance (NQR) measurements.[1,2] The salient features of the phase diagram are: (i) a line of paramagnetic (PM) to antiferromagnetic (AF) transitions

which starts at the Néel temperature $T_N \approx 300$ K for $x=0$ and drops rapidly to $T_N \approx 0$ for $x \approx 0.02$; (ii) in the same concentration range $0<x<0.02$, a line of spin freezing of the transverse Cu^{2+} spin distortions (generated by doped holes localized around Sr impurities) into a spin-glass-like state which is superimposed on the antiferromagnetic background and is described by $T_f \approx (815\ \text{K})x$; and (iii) a line of PM to cluster spin-glass transitions which goes as $T_g \propto 1/x$ for the concentration range $0.02 \leq x \leq 0.05$. The second feature of the phase diagram was explained quantitatively by a simple classical model[3] mimicking the spin distortions generated by doped holes which are assumed to be localized in the CuO_2 plane near Sr^{2+} impurity ions.[4] Here we present a variety of new experimental data further detailing the magnetic state of this system, and present a simple theory of the Cu^{2+} staggered magnetization $M^\dagger$ that quantitatively agrees with experiment.

The detailed temperature dependence of M^* (i.e., the order parameter) in the different regions of the T-x plane of the phase diagram is of interest for understanding the microscopic mechanism by which the magnetic properties are affected by the hole doping. Previous studies[5,6] have shown how $M^\dagger$ behaves as a function of temperature and excess oxygen levels in $La_2CuO_{4+\delta}$, but the previous work has not led to a comprehensive understanding of how Sr doping affects the order parameter in $La_{2-x}Sr_xCuO_4$. In this paper, we study how the mobile holes introduced by Sr impurities affect $M^\dagger(x,T)$ and show that the result is very different than has been obtained for $La_2CuO_{4+\delta}$ samples with $T_N \sim 100$ K. To be specific, excess oxygen doping produces reentrant behavior below ≈ 25 K,[5] where $M^\dagger$ *decreases* with decreasing T, and it has been proposed in Ref. 6 that this phenomenon can be explained if one assumes that the mobile excess oxygen holes affect the spin ordering much less than do localized carriers. In this report, we will show that mobile holes introduced by Sr impurity ions produce a far move substantial reduction of $M^\dagger(x,T)$ than do these carriers below their localization transition. In particular, measurements of the Zeeman splitting $\Delta\nu$ ($\sim H_{\text{int}} \sim M^\dagger$) of the ^{139}La NQR in $La_{2-x}Sr_xCuO_4$ (which are carried out in zero applied magnetic field H) show[1] an anomalous temperature dependence of the local internal magnetic field H_{int} in the doping range $0<x<0.02$ (see Fig. 1): the addition of Sr decreases H_{int} in the temperature interval from $T_N(x)$ down to 30 K, while below this temperature, H_{int} *increases* again and in the limit of $T \to 0$, H_{int} is practically independent of Sr concentration. The upturn of H_{int} below 30 K for $0<x<0.02$ was tentatively ascribed to the localization of the holes introduced by Sr doping,[1] but otherwise a comprehensive description of this anomalous behavior of $H_{\text{int}}(x,T)$ and $M^\dagger(x,T)$ in the above concentration range was not produced.

The Zeeman splitting of the ^{139}La NQR line depends on both the magnitude and the local orientation of $\mathbf{H}_{\text{int}}$ with respect to the electric-field gradient (EFG) principal axis, and therefore may not be simply proportional to $M^\dagger(x,T)$. Thus, in order to get an unambiguous determination of $M^\dagger(x,T)$, we performed zero-field positive muon spin rotation (μSR) measurements on the same set of samples used for the NQR measurements to get the local field magnitude at the muon site. Furthermore, we performed ^{139}La nuclear magnetic resonance (NMR) measurements on a La_2CuO_4 single crystal to measure the temperature dependence of the orientation of the EFG principal axis with respect to the crystalline pseudotetragonal c axis. Thus, by combining the NQR, the NMR, and the μSR measurements, we have deduced that the temperature dependences in Fig. 1 arise mainly from $M^\dagger(x,T)$.

The reduction of $M^\dagger$ when the system is doped with Sr was qualitatively ascribed[1,7] to the reduction of the dimensionality of the system as a consequence of the microsegregation of the electronic holes with the consequent formation of AF domains.[2,8] Here, we will address the problem quantitatively by using conventional spin-

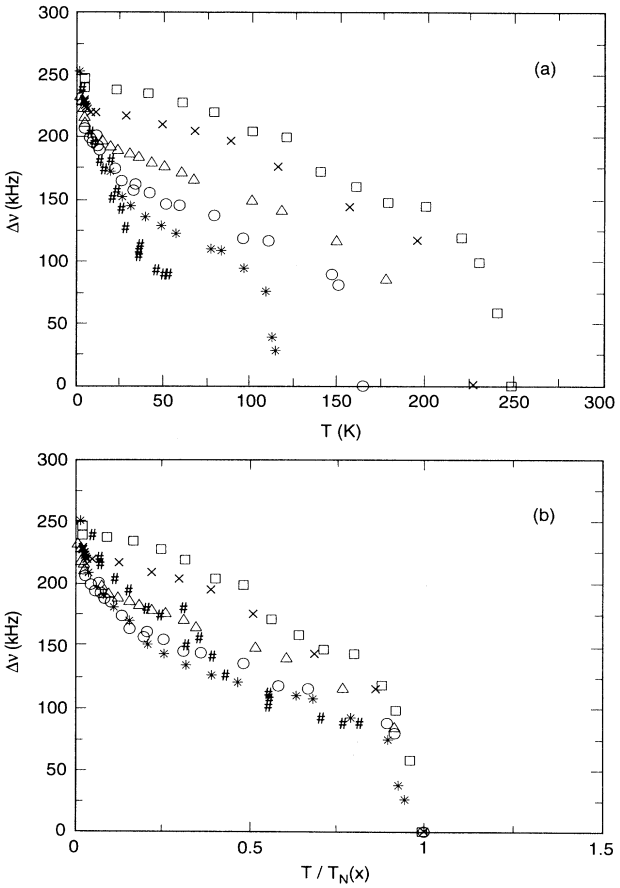

FIG. 1. Zeeman frequency splitting $\Delta\nu$ versus (a) temperature T and (b) reduced temperature $T/T_N(x)$, where $T_N(x)$ is the composition-dependent Néel temperature in Table I, of the $2\nu_Q$ ^{139}La NQR line at 12 MHz in $La_{2-x}Sr_xCuO_4$. Symbols: (□) $x=0$; (×) $x=0.008$; (△) $x=0.012$; (○) $x=0.014$; (*) $x=0.016$; (#) $x=0.018$. The data for the first five samples are from Ref. 1, whereas those for the last sample are from the present work.

wave theory[9] to calculate $M^{\dagger}(x,T=0)$ where we assume a simple model of mobile doped holes which move in a given CuO_2 plane in "rivers" which separate undoped AF regions, making the crystal look as if it was a collection of AF stripes of infinite length and finite width. This model is consistent with the phase separation phenomenology of mobile carriers in AF systems proposed by Emery and Kivelson.[10]

The paper is organized as follows. In Sec. II we give details about the sample preparation and about the experimental methods. In Sec. III we briefly review the theory for the μSR and ^{139}La NQR and NMR spectra. In Sec. IV, we present the data for the NMR in single crystal La_2CuO_4 from which we derive the temperature-dependent tilt angle of the CuO_6 octahedra. The measured tilt angle is discussed in conjunction with the NQR splitting to obtain information about the temperature dependence of the direction of $\mathbf{H}_{\rm int}$. In Sec. V we present the measurements of $M^{\dagger}(T)$ in $La_{2-x}Sr_xCuO_4$ as a function of x from both NQR and μSR measurements. In Sec. VI we present a simple model that we have used to calculate the reduction of $M^{\dagger}(x,T)$ due to finite-size effects. Considering their simplicity, the calculations give surprisingly good agreement with the data, and strongly support the hypothesis of hole microsegregation[1,2,8] in the doping range $0<x<0.02$. In Sec. VII we discuss the low-temperature data ($T<30$ K) and show that they are qualitatively consistent with the hypothesis of hole localization. Finally in Sec. VIII we provide a summary of our results and restate our conclusions.

II. EXPERIMENTAL DETAILS

Powder samples of nominal composition $La_{2-x}Sr_xCuO_4$ were prepared by conventional solid-state reaction at 925 and 1050 °C using predried high purity ($\geq 99.99\%$) La_2O_3, $SrCO_3$, and CuO, in x increments of 0.002 from $x=0$ to 0.03.[1,2,8] The homogeneity of the samples was insured by frequent and thorough grinding. For each composition, the final single phase product was separated into three parts which were treated at 650 °C for 5 h in 1 bar O_2; 1 bar N_2, and 200 bar O_2 atmospheres, respectively. Differential scanning calorimetry measurements confirmed the Sr doping levels and homogeneity from the agreement of $T_{T/O}(x)$ for the 1 bar N_2 annealed series with that obtained in Refs. 2 and 11, where $T_{T/O}$ is the tetragonal-to-orthorhombic transition temperature. The (average, see below) T_N was determined to about ± 5 K from the peak of $\chi(T)$ measured with a superconducting quantum interference device (SQUID) magnetometer.[2] The present measurements were carried out on the 1 bar O_2-annealed series of samples. Our previous study in Ref. 2 of $T_N(x)$ for the 1 bar N_2-annealed, 1 bar O_2-annealed, and 200 bar O_2-annealed series ($0\leq x\leq 0.02$) showed that each series followed the same behavior, namely $T_N(x)=T_N(0)[1-(x/x_c)^n]$ ($n\approx 2$), where the curves for each series were nearly parallel and shifted monotonically with oxygen pressure during annealing. These results indicate that for a given series the oxygen content is independent of the Sr content x (as also indicated by thermogravimetric analysis measurements[2]) and that x is an accurate measure of the change in the doped hole concentration in CuO_2 planes from that at $x=0$.

The La_2CuO_4 single crystal was grown by the CuO flux growth method. The crystal was annealed in Ar atmosphere at 600 °C for 10 h. The Néel temperature measured by susceptibility on a SQUID magnetometer was $T_N=308$ K. Two single crystals, each of $14\times 14\times 1$ mm^3 size, were stacked together with a common c axis to increase the ^{139}La NMR signal-to-noise ratio.

The NMR and NQR measurements were performed with a phase coherent Fourier Transform (FT) pulse spectrometer. The ^{139}La NQR was performed mostly on the $2\nu_Q$ ($\pm 5/2\leftrightarrow\pm 3/2$) transition occurring in the frequency range $\nu\approx 12$–13 MHz. Below T_N the line is split into two components, separated by $\Delta\nu$ in frequency, by the spontaneous local internal field $\mathbf{H}_{\rm int}$. At low temperatures, where $\Delta\nu$ is large, the NQR spectrum was determined by plotting the integrated echo intensity as a function of the transmitter frequency. A sample spectrum is shown in Fig. 2. For higher temperatures, when $\Delta\nu$ is reduced to less than 100 kHz, the signal can be obtained directly from the FT of half of the echo signal. In all cases the frequency spectrum was fitted with the sum of two Gaussian functions of equal intensity to derive the value of the splitting $\Delta\nu$ and of the full width at half maximum (FWHM).

The ^{139}La NMR measurements on the La_2CuO_4 single crystal were performed at an applied magnetic field $H=8.2$ T corresponding to a Larmor frequency $\nu_L=49.31$ MHz. The ^{139}La NMR spectrum was obtained directly by Fourier transformation of half of the echo.

Zero-field μSR measurements were performed at Rutherford Appleton Laboratory on the EMU beamline using 100% spin-polarized 29 MeV/c muons. The time evolution of the muon polarization was detected over an interval of 16 μs. The spurious signal due to cryostat walls and silver shieldings was previously calibrated by replac-

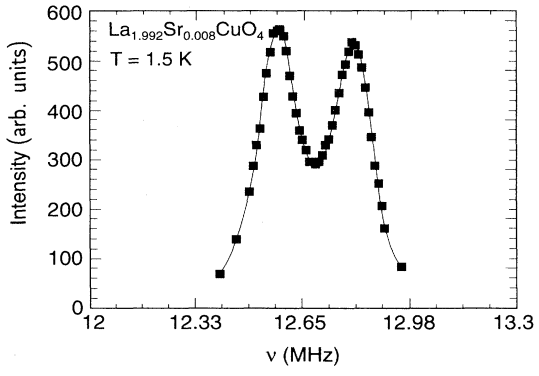

FIG. 2. Example of ^{139}La NQR spectrum (the $2\nu_Q$ line) showing the Zeeman splitting at 1.5 K due to the local internal magnetic field $\mathbf{H}_{\rm int}$. The spectrum is obtained by plotting the integrated echo intensity as a function of transmitter frequency.

ing the $30\times30\times2$ mm^3 powder sample with natural hematite which provides no signal. The fraction of nonprecessing muons below T_N was estimated by applying a 100 G transverse field B_T. This field strongly overdamps the signal from muons precessing around the internal field. Thus, only muons precessing at the frequency $\omega_\mu=\gamma_\mu B_T$ are observed: those associated with the previously calibrated spurious signal and those which have stopped in nonordered microscopic regions.

III. THEORETICAL BACKGROUND FOR THE NQR, NMR, AND μSR MEASUREMENTS

The ^{139}La NQR and NMR spectra are complicated by the simultaneous presence of strong quadrupole interactions and of a spontaneous local internal magnetic field $\mathbf{H}_{\rm int}$ below T_N.[12,13] The NQR spectrum is composed of three lines at ν_Q, $2\nu_Q$, and $3\nu_Q$, respectively. The asymmetry parameter is very small [$\eta\approx0.02$ (Refs. 13–15)] and we will thus approximate it by zero in the following. In the presence of $\mathbf{H}_{\rm int}$, the two lines at $2\nu_Q$ and $3\nu_Q$ each split into a doublet with frequency separation $\Delta\nu$ given by

$$\Delta\nu=\frac{2\gamma}{2\pi}H_{\rm int}\cos\zeta=\frac{2\gamma}{2\pi}H_{\rm int}^{\parallel}\ , \tag{1}$$

where γ is nuclear gyromagnetic ratio, and ζ is the angle between $\mathbf{H}_{\rm int}$ and the principal axis z' of the EFG (see Fig. 3). The lowest frequency transition at $\nu_Q(\pm1/2\leftrightarrow\pm3/2)$, on the other hand, gives rise to two doublets since the admixture of Zeeman states allows transitions with differences of azimuthal quantum number $\Delta m=\pm2$. The frequencies of the four lines are given by[13]

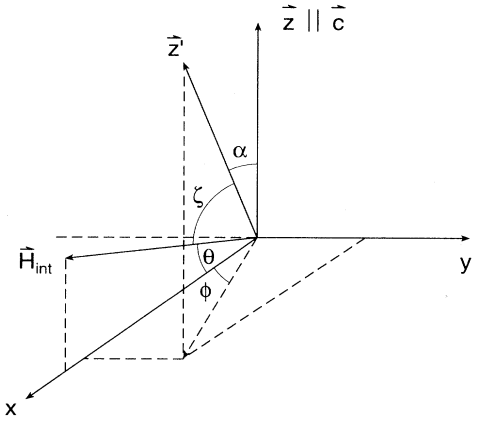

FIG. 3. Diagram defining the orientation of the EFG principal axis, z', and of the internal field $\mathbf{H}_{\rm int}$ with respect to the crystalline c axis and a-b plane.

$$\begin{aligned}\nu_{2,1}&=\nu_Q\pm(3/2)\frac{\gamma}{2\pi}H_{\rm int}^{\parallel}\\&\quad-(1/2)\frac{\gamma}{2\pi}\sqrt{(H_{\rm int}^{\parallel})^2+(4H_{\rm int}^{\perp})^2}\ ,\\ \nu_{4,3}&=\nu_Q\pm(3/2)\frac{\gamma}{2\pi}H_{\rm int}^{\parallel}\\&\quad+(1/2)\frac{\gamma}{2\pi}\sqrt{(H_{\rm int}^{\parallel})^2+(4H_{\rm int}^{\perp})^2}\ ,\end{aligned} \tag{2}$$

where we see that the splitting of the NQR line at ν_Q depends on both the components of $\mathbf{H}_{\rm int}$ parallel and perpendicular to the EFG principal axis.

In order to measure the magnitude of $\mathbf{H}_{\rm int}$ [which should be approximately proportional to $M^{\dagger}(x,T)$] below T_N from NQR, ideally one should measure the positions of the four low-frequency ν_Q lines and use Eq. (2). This was done successfully in a good single crystal of La_2CuO_4,[14] measurements which we did not repeat. In Sr-doped samples, we found it impossible to follow this method due to the additional broadening introduced by the random distribution of Sr ions in the lattice. Thus one has to get the internal field from the splitting of the $2\nu_Q$ or $3\nu_Q$ line and use Eq. (1), which yields only the component $H_{\rm int}^{\parallel}$ parallel to the EFG principal axis.

In the NMR regime at high fields ($\gamma H\gg\nu_Q$), one expects a ^{139}La spectrum which contains a central transition line ($+1/2\leftrightarrow-1/2$) and three pairs of satellite transitions involving these and/or the other six m levels. The shift $\delta\nu_Q$ of the central line with respect to the Larmor frequency $\nu_L=\gamma H/2\pi$ (for $\eta=0, I=7/2$ and in second-order perturbation theory) is

$$\delta\nu_Q=(15\nu_Q^2/16\nu_L)(1-\cos^2\alpha)(1-9\cos^2\alpha)\ , \tag{3}$$

where the tilt angle α is the angle between the principal z' EFG axis and the c axis, the defined in Fig. 3. In the presence of an internal field forming an angle $\pi/2-\theta$ with the crystalline **c** axis, see Fig. 3, and with the external field $\mathbf{H}\|\mathbf{c}$, one has

$$\delta\nu=\delta\nu_Q+\frac{\gamma}{2\pi}H_{\rm int}\sin\theta=\delta\nu_Q+\frac{\gamma}{2\pi}H_{\rm int}^{z}\ , \tag{4}$$

where $H_{\rm int}^{z}$ is the component of $\mathbf{H}_{\rm int}$ in the direction of the **c** axis.

The muon polarization signal in our μSR measurements, arising from muons stopped in the sample, was fitted according to[16]

$$P_\mu(t)=A_1e^{-\sigma t}\cos(\gamma_\mu B_\mu t+\phi)+A_2e^{-\lambda t}\ , \tag{5}$$

where $\gamma_\mu/2\pi=135.5$ MHz/T is the muon gyromagnetic ratio, B_μ the local field at the muon site, and σ and λ the transverse and longitudinal decay rates, respectively. The two components on the right-hand side of Eq. (5) originate from the average over solid angle of the $\mathbf{B}_\mu$ components transverse and parallel to the initial muon polarization, respectively. In principle, one should find $A_1\approx2A_2$. However, due to different effects, the A_1/A_2 ratio is modified. Namely, the finite temporal width of the muon beam pulses causes a reduction in the amplitude of the oscillatory signal (A_1) which is a function of

B_μ and therefore of the temperature. Furthermore, due to the increasing "nonmagnetic" fraction for $T \to T_N$ (see below), one observed an enhancement of A_2 with temperature. The relationship $\sigma < \gamma_\mu B_\mu$ was observed to hold over the whole temperature range, thus allowing a meaningful estimate of B_μ. Only one muon site and no evidence of muon diffusion were detected. The estimate of λ was carried out for $x = 0.008$ only at low temperatures, where the nonmagnetic fraction is small. Due to the fast damping of the oscillatory signal ($\sigma \approx 1.5\ \mu s^{-1}$), a fit to the decay of the polarization with a single exponential ($Ae^{-\lambda t}$, with A and λ as free parameters) over the last 14 μs of the histogram provided the estimate of λ.

IV. NQR, NMR, AND μSR SPECTRA FOR $La_2CuO_{4+\delta}$: THE LOCAL INTERNAL MAGNETIC FIELD

For an applied field $\mathbf{H} \| \mathbf{c}$ in a single crystal with the crystalline structure of La_2CuO_4, one expects to have two La sites with opposite directions of $\mathbf{H}_{int}$. From Eq. (4), this should result, below T_N, in a splitting of the NMR line. However, since $\mathbf{H}_{int}$, lies very nearly in the *ab* plane,[13] the splitting from Eq. (4) is expected to be small and within the NMR width. For $T = 46$ K, we indeed observed that the ^{139}La NMR line for a La_2CuO_4 crystal ($T_N = 308$ K) with $\mathbf{H} \| \mathbf{c}$ is symmetric, showing no evidence for a splitting, with a FWHM of about 115 kHz. Thus, $\delta\nu$ in Eq. (4) is the same as $\delta\nu_Q$ in Eq. (3) to within our resolution. Since the splitting should be less than half of the FWHM in order not to be observable, we obtained an upper limit $\theta \leq 2.5°$ for the angle formed by $\mathbf{H}_{int}$ with the *ab* plane (see Fig. 3), assuming[13] $H_{int} = 1000$ G in Eq. (4).

Our μSR measurements were carried out on a powder sample of $La_2CuO_{4+\delta}$. The *magnitude* of the local magnetic field at the muon site, B_μ, was determined at each T according to Eq. (5), and its T dependence is included in Fig. 9(b) below. The T dependence of the normalized local field magnitude, $B_\mu(T)/B_\mu(0)$, is plotted in Fig. 4. For comparison, also plotted in Fig. 4 are (i) the normalized *magnitude* of the local field at the La site, $H_{int}(T)/H_{int}(0)$, obtained from the four T-dependent NQR frequencies at ν_Q given in Ref. 14 for a crystal with $T_N = 318$ K, using Eqs. (2); (ii) the normalized *parallel component* of the local field at the La site, $H^{\|}_{int}(T)/H^{\|}_{int}(0)$, obtained from the same measurements and crystal as in (i), again using Eqs. (2); and (iii) the normalized *parallel component* of the local field at the La site, $H^{\|}_{int}(T)/H^{\|}_{int}(0)$, obtained from the T-dependent Zeeman splitting $\Delta\nu$ of the NQR line at $2\nu_Q$ in Fig. 1 (Ref. 1) for the $x = 0$ sample, using Eq. (1).

From Fig. 4, we first note the rather good agreement between the T dependences of $B_\mu(T)/B_\mu(0)$ and $H_{int}(T)/H_{int}(0)$; the two measurements of $H^{\|}_{int}(T)/H^{\|}_{int}(0)$ are also in good agreement with each other. However, the T dependence of $H^{\|}_{int}(T)/H^{\|}_{int}(0)$ is significantly different from that of $B_\mu(T)/B_\mu(0)$ and $H_{int}(T)/H_{int}(0)$. Referring to Fig. 3 and Eqs. (1) and (2), this disagreement must mean the angle ζ between $\mathbf{H}_{int}$

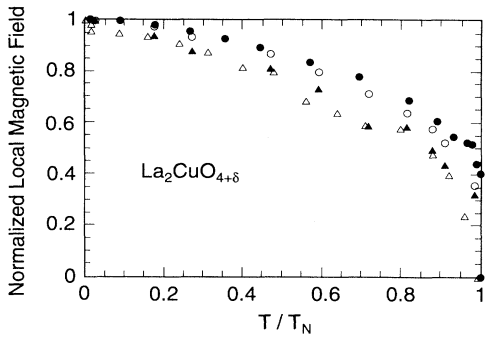

FIG. 4. Local internal magnetic field, normalized to the zero-temperature value, versus reduced temperature T/T_N for $La_2CuO_{4+\delta}$: (●) magnitude of the internal field from our μSR data $B_\mu(T)/B_\mu(0)$($T_N = 280$ K); (○) magnitude $H_{int}(T)/H_{int}(0)$ of the internal field from the ^{139}La NQR data in Ref. 14 analyzed according to Eq. (2) in the text ($T_N = 318$ K); (△) parallel component $[H^{\|}_{int}(T)/H^{\|}_{int}(0)]$ of the local internal magnetic field from the Zeeman splitting $\Delta\nu$ in Fig. 1 (Ref. 1) of the NQR line at $2\nu_Q$ using Eq. (1) for the $x = 0$ sample with $T_N = 250$ K; (▲) $H^{\|}_{int}(T)/H^{\|}_{int}(0)$ from the Zeeman splitting of the ν_Q line (from Ref. 14) ($T_N = 318$ K).

and the EFG principal z' axis depends on temperature. The temperature dependence of ζ can arise from a T dependence of the orientation of the EFG principal (z') axis with respect to the crystal axes and/or from a T dependence of the orientation of $\mathbf{H}_{int}$ (see Fig. 3). We studied the former effect by measuring the angle α, which is the angle between the local EFG principal z' axis and crystalline c axis (see Fig. 3), from the shift $\delta\nu_Q$ of the central NMR transition [see Eq. (3)] in a La_2CuO_4 single crystal ($T_N = 308$ K) aligned with the c axis along the external field. For this orientation the six satellites are far removed in frequency and do not interfere with the measurements. The results are shown in Fig. 5, where α

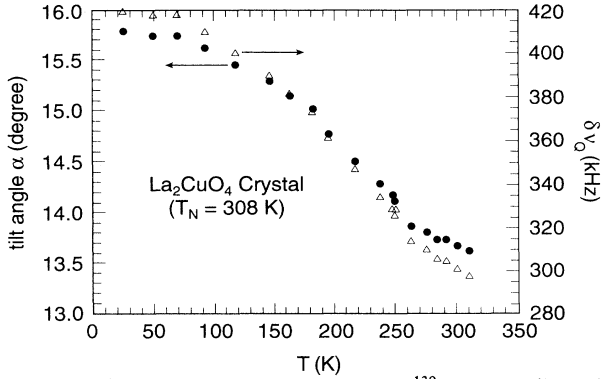

FIG. 5. (△) the shift $\delta\nu_Q$ of the central ^{139}La NMR line with respect to the calculated Larmor frequency in an external field of 8.2 T for a La_2CuO_4 crystal with $T_N = 308$ K, versus temperature T. (●) Angle α between the local EFG principal axis (z' axis in Fig. 3) and the crystalline c axis vs T, obtained from the $\delta\nu_Q(T)$ data using Eq. (3).

is seen to increase from 13.6° to 15.8° upon cooling from 308 to 23 K. The angle is zero for perfect local tetragonal symmetry while it becomes different from zero below the tetragonal to orthorhombic transition [occurring in stoichiometric La_2CuO_4 at about 530 K (Ref. 11)]. It is believed that the tilting of the z' axis is a consequence more of a lateral displacement of the apical oxygen atoms rather than of the rigid rotations of the CuO_6 octahedra which are responsible for the structural transition.[15] Although the absolute value of the angle can be affected by a systematic error of order of 2° due to the use of the Eq. (3) based on second-order perturbation theory and due to misalignment of **H** with respect to **c**, its relative temperature dependence is meaningful.

The temperature dependence of the angle ζ can be directly obtained experimentally from the splitting of the NQR line at ν_Q using Eqs. (2), since $\tan\zeta = H_{\rm int}^{\perp}/H_{\rm int}^{\parallel}$. Using the data in Ref. 14, ζ vs T was determined and is plotted in Fig. 6. From the relation

$$\cos\zeta(T)=\sin\alpha(T)\cos\phi(T)\cos\theta(T)+\sin\theta(T)\cos\alpha(T)\ , \tag{6}$$

where the angles θ and ϕ are defined in Fig. 3, one can see that the T dependence of ζ can come from several sources. We calculated the T dependence of ζ from the experimental results for $\alpha(T)$ in Fig. 5 by keeping θ and ϕ fixed. The results, shown in Fig. 6, indicate that the T dependence of α, taken alone, cannot be responsible for all of the T dependence of ζ. On the other hand, one can obtain good agreement between the experimental and the calculated $\zeta(T)$ if one also allows for a T dependence of ϕ. For example, for fixed θ in the range 1° to 3°, we found good agreement by choosing $\phi \approx 45°$ and allowing for a temperature variation in ϕ of the order of 5° to 8° in the range of interest. It is also possible to get solutions for fixed ϕ and a $\theta \sim 2°$ which varies with temperature by about 1°. We conclude that the differences between $H_{\rm int}^{\parallel}$ (as measured in NQR) and $H_{\rm int}$ (as measured in μSR or with the ν_Q lines in NQR as in Fig. 4) should mainly be ascribed to the T dependence of the tilt angle α with a small contribution coming from the temperature dependence of the orientation of $\mathbf{H}_{\rm int}$ with respect to the c axis (i.e., the angle θ in Fig. 3), or of the mutual orientation of the projections of $\mathbf{H}_{\rm int}$ and $\mathbf{z}'$ onto the xy plane (angle ϕ in Fig. 3); these two effects cannot be distinguished on the basis of our measurements.

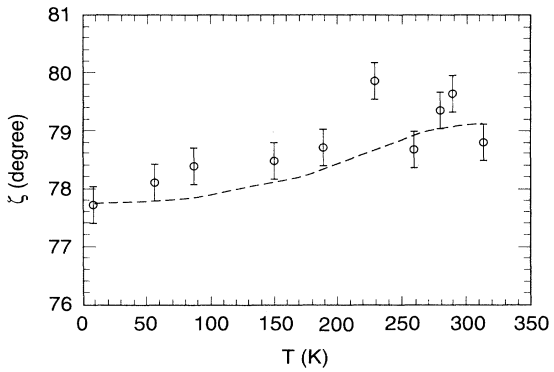

FIG. 6. Angle ζ between $\mathbf{H}_{\rm int}$ and the z' axis (see Fig. 3) vs temperature T in the La_2CuO_4 single crystal ($T_N = 318$ K): (○) values obtained from the experimental data in Ref. 14 by using Eq. (1) as explained in the text; (— — —) theoretical estimate obtained by using the relation [Eq. (6)] between the angle ζ and the angles α, θ, and ϕ, where for $\alpha(T)$ we used the experimental data in Fig. 5, while the other two angles were held constant at $\theta = 2°$ and $\phi = 47°$.

V. EFFECT OF Sr DOPING ON THE STAGGERED MAGNETIZATION OF $La_{2-x}Sr_xCuO_4$

The anomalous T dependence of the Zeeman splitting $\Delta\nu$ of the $2\nu_Q$ ^{139}La NQR line in samples with different concentration x of Sr was shown above in Fig. 1 and briefly discussed in the Introduction. As shown in the previous paragraph, the anomalous T dependence of $H_{\rm int}^{\parallel}$ below 30 K could arise from that of either the magnitude or orientation of $\mathbf{H}_{\rm int}$ or from both. Therefore, we performed measurements of the local-field magnitude at the muon site from zero field μSr in the same samples that were used in the ^{139}La NQR study.[1] The results, shown in Fig. 7, when compared to the NQR results in Fig. 1, clearly indicate that the main anomalous features are similar in both sets of data. This demonstrates that the anomalous T dependence below ≈ 30 K arises mostly from the behavior of the staggered magnetization since this would affect both kinds of measurements in the same way. The remaining small differences between $\Delta\nu(T)/\Delta\nu(0)$ and $B_\mu(T)/B_\mu(0)$ have to be ascribed to the temperature dependence of the orientation of the internal field which affects only the NQR data [see Eq. (1)].

In Fig. 8 we show the fraction f of muons experiencing zero local field as a function of temperature. For $x > 0$ there is a finite temperature interval below T_N in which muons experiencing a local internal field and zero field coexist. The distribution of internal fields just below T_N suggests the presence in the doped samples of a distribution of Néel temperature T_N. It is noted that the distribution of internal fields near T_N could not be observed in the NQR experiment because it would give rise to additional broadening smaller than the quadrupole broadening of the NQR line.

We turn now to the analysis of the data in Figs. 1 and 7 based on the following working hypothesis: (i) the temperature dependence of the staggered magnetization $M^{\dagger}(x,T)$ above 30 K is described by a power law:

$$M^{\dagger}(x,T)/M^{\dagger}(x,0)=[1-T/T_N(x)]^{\beta}\ , \tag{7}$$

where β is assumed to be independent of x, while T_N and the extrapolated $T=0$ saturation values of the staggered magnetization $M^{\dagger}(x,0)$ are functions of Sr doping; (ii) the anomalous increase of the internal field below 30 K is ascribed to changes in the mobility of the electronic holes, as discussed in Sec. VII below, and will thus be excluded in the fitting of the data; (iii) the relative temperature

dependences $\Delta\nu(x,T)/\Delta\nu(x,0)$ and $B_\mu(x,T)/B_\mu(x,0)$ are both direct measures of the reduced staggered magnetization in Eq. (7). The fits of Eq. (7) to the data in Figs. 1(a) and 7(a) are shown in Figs. 9(a) and 9(b), respectively. The extrapolated values of the fits at $T\rightarrow 0$ yield the x dependence $M^\dagger(x,0)/M^\dagger(0,0)$. The temperature dependence of the reduced magnetization in Eq. (7) is obtained separately from $\Delta\nu(T)/\Delta\nu(0)$ and from $B_\mu(T)/B_\mu(0)$. The two sets of data give somewhat different values for the parameters β and $T_N(x)$ as shown in Tables I and II. The difference in β values is due to the effect of the T dependence of the orientation of $\mathbf{H}_{\rm int}$ discussed previously. The differences in T_N in Tables I and II for a given x value are larger than the experimental errors. One contributing factor is that the μSR measurements yield the highest T_N present in a sample (see Fig. 8), whereas the NQR and susceptibility data yield the average T_N. Finally, the μSR measurements were done about one year after the NQR measurements. During this time, the average T_N was found to have increased for the lowest x samples. After the μSR measurements were completed, the aver-

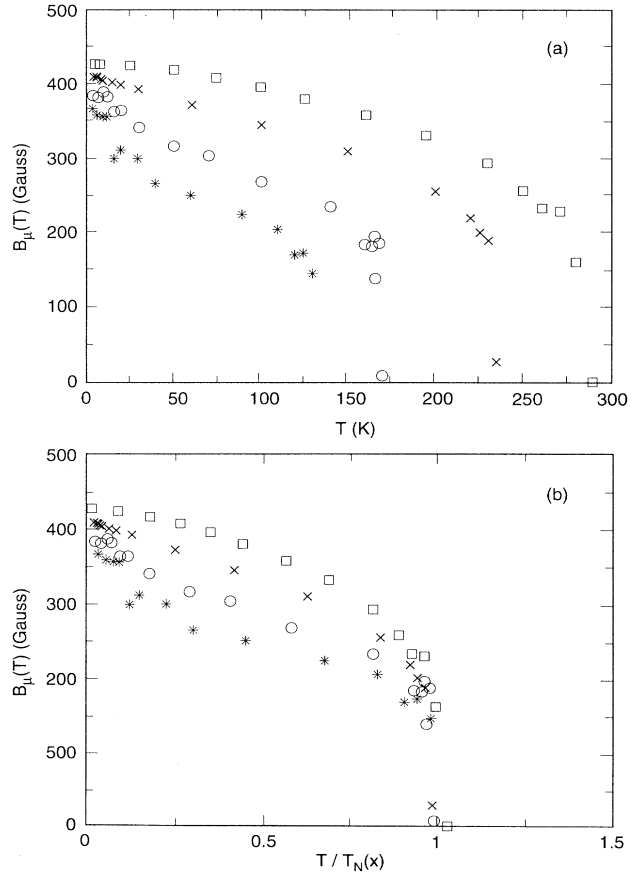

FIG. 7. Local internal field at the muon site B_μ in $La_{2-x}Sr_xCuO_4$ versus (a) temperature T and (b) reduced temperature $T/T_N(x)$, where the Néel temperatures $T_N(x)$ are given in Table II. Symbols: (□) $x=0$; (×) $x=0.008$; (○) $x=0.014$; (*) $x=0.016$.

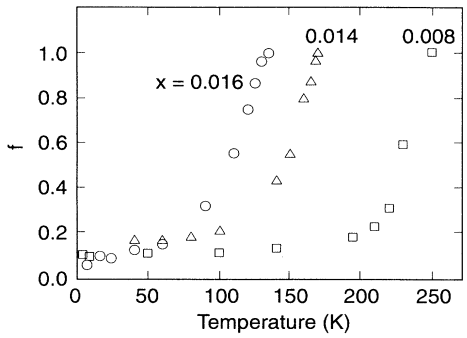

FIG. 8. Fraction f of muons experiencing zero local internal magnetic field vs temperature in $La_{2-x}Sr_xCuO_4$ for three different Sr concentrations x.

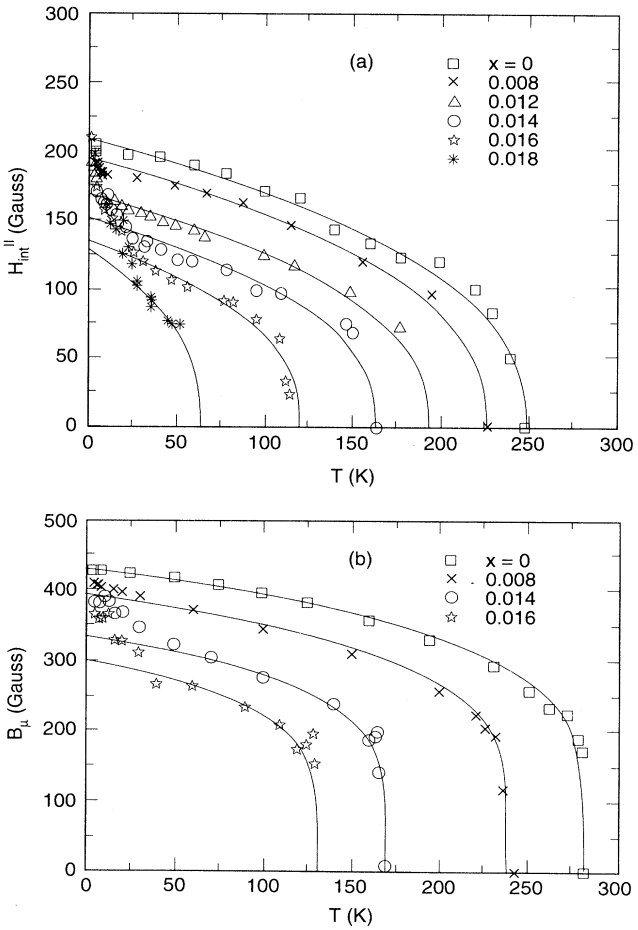

FIG. 9. Internal field $H_{\rm int}^{\parallel}$ (a) and B_μ (b) vs temperature T in $La_{2-x}Sr_xCuO_4$ for different Sr concentrations x. In (a), the experimental points are derived from the NQR data in Fig. 1(a) using Eq. (1). The full lines are best-fit curves according to Eq. (7) in the text where only the data for $T>30$ K have been used in the fit. The best fit parameters are summarized in Table I. In (b), the experimental points are the same μSR data shown in Fig. 7(a). The full lines are the best-fit curves according to Eq. (7) in the text where only the data for $T>30$ K have been used in the fit. The best-fit parameters are summarized in Table II.

TABLE I. Summary of the parameters for $La_{2-x}Sr_xCuO_4$ obtained from the fit of Eq. (7) to the NQR data in Fig. 9(a) as explained in the text. The values of $T_N(x)$ in this table are the same as the ones determined independently from static magnetic susceptibility and ^{139}La NQR measurements (Refs. 1 and 2).

x	$\Delta\nu(x,0)$ (kHz)	$H_{int}^{\parallel}(x,0)$ (G)	β	$T_N(x)$ (K)
0	251.4	418	0.41	250
0.008	234.7	390	0.41	227
0.012	202.9	337	0.41	194
0.014	182.1	303	0.41	164
0.016	162.7	270.5	0.41	121
0.018	154.6	257	0.41	64

age T_N of the $x=0$ and 0.008 samples was found from susceptibility measurements to be ≈ 270 and ≈ 233 K, respectively. Since our analyses are carried out in terms of reduced temperature $T/T_N(x)$, these shifts in T_N over time do not affect our conclusions.

For the purpose of determining the reduction of the reduced staggered magnetization with increasing x extrapolated to $T=0$, the two sets of data give very similar results. This is shown in Fig. 10 where the data in Tables I and II are plotted together with a curve of best fit given by

$$\Delta\nu(x,0)/\Delta\nu(0,0)=B_\mu(x,0)/B_\mu(0,0)$$
$$=M^\dagger(x,0)/M^\dagger(0,0)=(1-x/x_c)^n \quad (8)$$

with $n=0.236$ and $x_c=0.023$. The right-hand side of Eq. (8), chosen to fit the data, is purely empirical. It suggests that in the absence of the hole localization occurring below ≈ 30 K (see below), the order parameter $M^\dagger(x,0)$ is reduced by quantum fluctuations via nonzero Sr concentration x, in a way similar to the reduction of the order parameter by thermal fluctuations [see Eq. (7) and Fig. 9]. The hypothesis adopted previously[1,2,7,8] and below is that the effect of Sr doping is to generate finite-size domains with average local staggered moment reduced by the enhancement of the fluctuations due to finite-size effects. For example, the presence of finite-size

TABLE II. Summary of the parameters for $La_{2-x}Sr_xCuO_4$ obtained from the fit of Eq. (7) to the μSR data in Fig. 9(b) as explained in the text. The uncertainty in the values of the best-fit parameters listed both in the present table and in Table I is best assessed by the direct visual comparison of the fitting curves with the experimental data in Figs. 9(a) and 9(b).

x	$B_\mu(x,0)$ (G)	β	$T_N(x)$ (K)
0	430.3	0.21	280
0.008	393.8	0.21	238
0.014	335	0.21	171
0.016	300	0.21	132

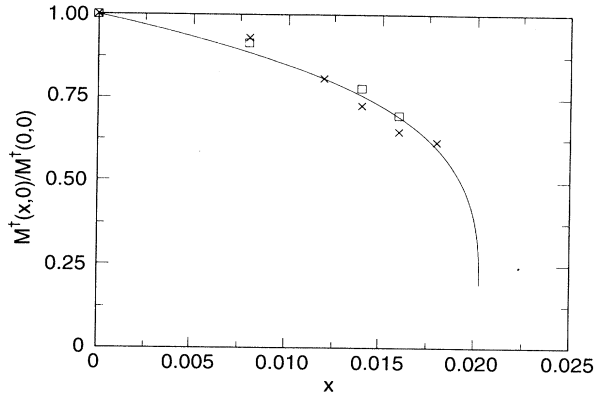

FIG. 10. Normalized zero-temperature staggered magnetization $M^\dagger(x,0)/M^\dagger(0,0)$ as a function of Sr concentration x in $La_{2-x}Sr_xCuO_4$, extrapolated from above 30 K using the fits in Fig. 9. The points are the best fit parameters shown in Tables I and II from NQR ($\times$) and from μSR ($\square$), respectively. The full line is the best-fit curve according to Eq. (8) in the text.

domains with a distribution of T_N values in the $x<0.02$ Sr-doped samples is corroborated by the gradual falloff observed below T_N in the fraction of muons experiencing zero local magnetic field (see Fig. 8). For $x>x_c=0.023$, T_N goes to zero. In the following section we provide detailed calculations of the staggered magnetization which show that this interpretative model to fit the data is a plausible one.

VI. A MODEL DEMONSTRATING FINITE-SIZE EFFECTS ON THE STAGGERED MAGNETIZATION BELOW T_N IN $La_{2-x}Sr_xCuO_4$

The basis of our model follows from the phenomenology that was proposed in Refs. 1, 2, and 8 to self-consistently explain the measured susceptibilities and NQR data as a function of doping. To be specific, it was proposed that for weakly doped $La_{2-x}Sr_xCuO_4$ below T_N, carrier-rich domain walls are formed, separating undoped spin-rich domains, and that these walls effectively reduce the dimensionality of the spin-rich regions in the CuO_2 planes. This phenomenology is consistent with the (frustrated) phase separation ideas of Emery and Kivelson.[10]

Figure 11 shows an idealized distribution of carriers in a CuO_2 plane, in which the holes in the domain walls are separated on average by a distance of S_h (in units of the planar lattice constant), and the walls are separated from one another by a distance of L (again, in units of a lattice constant). It is to be emphasized that the holes are in motion along the direction of these domain walls, and in what follows we approximate that the effect of this motion is to isolate the spin-rich domains from one another. This is a severe constraint, but one that (i) leads to good agreement with experiment, and (ii) can be re-

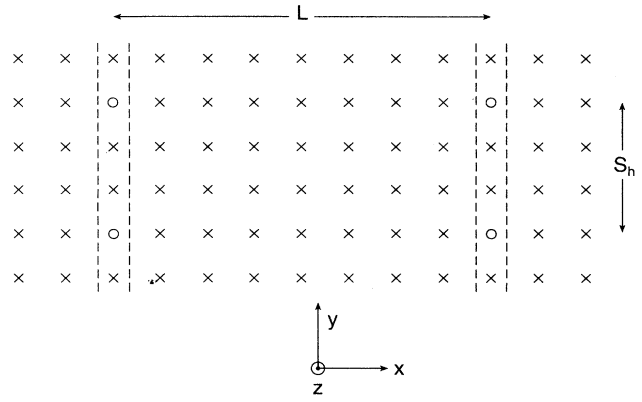

FIG. 11. Geometry of the domain walls, denoted by dashed lines, formed from microsegregated holes. The ×'s denote Cu spins, and the circles represent the holes. We focus on the limit $S_h \ll L$ in which the unidimensional geometry of the spin-rich domains is most apparent.

laxed in more realistic models of such planes (see below). Then, for a density of x holes in a given CuO_2 plane, one has

$$S_h \cdot L = \frac{1}{x} . \tag{9}$$

We consider a single spin-rich domain, infinite in extent in the y direction parallel to the domain walls, and then stack an infinite number of such regions one on top of another in the z direction; this provides us with a simple model of the spin degrees of freedom that are produced by such rivers of charge. Since we are concerned with the staggered magnetization *extrapolated* to $T=0$ from temperatures ($T > 30$ K) at which charge localization and anisotropies and asymmetric exchange interactions are largely unimportant,[5] we employ the simplest microscopic Hamiltonian describing the spins:

$$H = J_{\parallel} \sum_{\langle i,j \rangle} \mathbf{S}_i \cdot \mathbf{S}_j + J_{\perp} \sum_{\langle i,k \rangle} \mathbf{S}_i \cdot \mathbf{S}_k , \tag{10}$$

where the first sum is over all intraplanar nearest neighbors, and the second is over all interplanar nearest neighbors. In the following we utilize the experimental value[5] for the ratio ε of the Cu-Cu interplanar ($J_{\perp}$) to intraplanar ($J_{\parallel}$) exchange interactions in La_2CuO_4:

$$\varepsilon = J_{\perp}/J_{\parallel} \sim 5 \times 10^{-5} . \tag{11}$$

Then, using standard linear spin-wave theory[9] for spin-S spins, it is straightforward to show that the staggered magnetization at $T=0$, $M^{\dagger}(x,0)$, on a given Cu site in such an infinite stack (with tetragonal symmetry) of $L \times \infty$ domains is given by

$$M^{\dagger}(x,0) = S + \frac{1}{2} - \frac{1}{2(L-1)} \times \sum_{k_x} \frac{1}{(2\pi)^2} \int_{-\pi}^{\pi} dk_y \int_{-\pi}^{\pi} dk_z \frac{1}{\sqrt{1-\gamma_{\mathbf{k}}^2}} , \tag{12}$$

where

$$\gamma_{\mathbf{k}} = \frac{\cos k_x + \cos k_y + \varepsilon \cos k_z}{2+\varepsilon} . \tag{13}$$

In Eq. (12), the infinite extent of the spin lattice in the y and z directions manifests itself in the *integrals* over k_y and k_z, whereas the finite width of the lattice in the x direction requires that the k_x *discrete sum* be taken over only those wave vectors consistent with periodic boundary conditions.[17] Lastly, in Eq. (12) the carrier density x is related to the finite size L through Eq. (9).

We have fitted the data shown in Fig. 10 using Eq. (12) and fixing the one free variable S_h; for simplicity, and to minimize the number of free variables, we have chosen S_h to be independent of x. We find that $S_h = 5$ leads to good agreement with the data, and a comparison of our model and the data is shown in Fig. 12. Clearly, this agreement lends support for the presence of charge-rich domain walls in the AF phase; whether or not such domain walls, of any geometry, exist in non-AF phases at higher doping levels is an open question that we cannot address with these experiments.

Further predictions follow from the above model: The spin-correlation function at $T=0$ may be calculated, and to linear order we find that for two sites along the infinite direction of a planar domain

$$\langle (-1)^j \mathbf{S}(\mathbf{r}) \cdot \mathbf{S}(\mathbf{r} + j\hat{y}) \rangle \sim \frac{1}{j} , \tag{14}$$

in the limit of very large j. Thus, the spin correlations in the domains are, by definition, finite in extent along the domain width, and algebraic along the perpendicular direction. It would be interesting if two-axis neutron-scattering studies of $x < 0.02$ samples at low T could scrutinize this prediction. Also, we have considered the problem of the loss of unidimensionality implicit in Eq. (9) when $S_h \approx L$—then, a modified form of Eq. (9) immediately leads to a crossover from

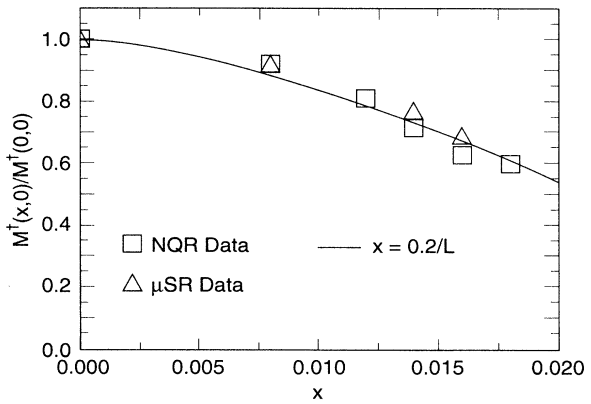

FIG. 12. The reduced staggered magnetization $M^{\dagger}(x,0)/M^{\dagger}(0,0)$ versus doping level x, produced from Eq. (12) using Eq. (9) to relate x to L, with $S_h = 5$ (solid curve), compared to the NQR and μSR values extrapolated from > 30 K, reproduced from Fig. 10.

$$L \sim \frac{1}{x} , \tag{15}$$

when $x < 0.02$, namely in the AF phase, to

$$L \sim \frac{1}{\sqrt{x}} , \tag{16}$$

when $x > 0.02$. This latter behavior has already been surmised from previous NQR studies[8] to describe the spatial extent of the domains in the cluster spin-glass phase, and the applicability of Eqs. (15) and (16) in the various regions of the magnetic phase diagram has already been discussed in Ref. 1. The theoretical details of this somewhat complicated crossover will be presented elsewhere.[18]

It is to be emphasized that the geometry of the spin-rich domains in Fig. 11 represents a severe restriction on spins, and one that is used for simplicity only. We wish to simply mimic the situation created by the mobile holes that are moving along one-dimensional rivers of charge. That this cannot be a completely accurate representation of the actual spin distributions is seen from a calculation of the doping dependence of the Néel ordering temperature: for a finite L, T_N drops immediately to zero quite simply because the system is now, in the renormalization-group sense, effectively a two-dimensional system, in conflict with experiment. The fully three-dimensional system with such rivers present will also produce the behavior of the staggered magnetization described in this paper, and should in addition describe the behavior of $T_N(x)$, a subject that we are now exploring.

An effect which has not been included in the above model is the distortions of the spin texture induced by the mobile carriers on the AF domains of spins. Since the mobile holes are quasiparticles which are known to induce long-range spin distortions of dipolar symmetry[19] one should, in principle, include the spin distortions in the calculation of the staggered magnetization. A preliminary calculation based on a highly simplified classical model and performed independently from the finite-size effect discussed above indicates that the reduction of the sublattice magnetization due to spin distortions is small compared to the quantum fluctuation effect.[18]

VII. HOLE LOCALIZATION IN $La_{2-x}Sr_xCuO_4$

As can be seen from the data in Figs. 1, 7, and 9, both the component $H_{\rm int}^{\parallel}$ and the magnitude B_μ increase abruptly below $T \approx 30$ K, reaching approximately the same x-independent values for $T \to 0$ in each case. This fact can be better appreciated in Fig. 13 where several low-temperature ($T \leq 4.2$ K) values of the Zeeman splitting $\Delta\nu \propto H_{\rm int}^{\parallel}$ from Fig. 1 and from additional measurements are plotted as a function of the Sr concentration x. The internal field is x and T independent for concentrations up to $x = 0.02$ and for $T \leq 4.2$ K. For $x > 0.02$, the AF phase disappears and a cluster-spin-glass phase is formed.[1,8] Thus, for $x > 0.02$ the x and T dependencies of the internal field are different and will not be discussed here. It should be noted by contrast that in the case of substitution of Cu with Zn in the CuO_2 plane, the anomalous T dependence of the staggered magnetization below 30 K is totally absent.[20]

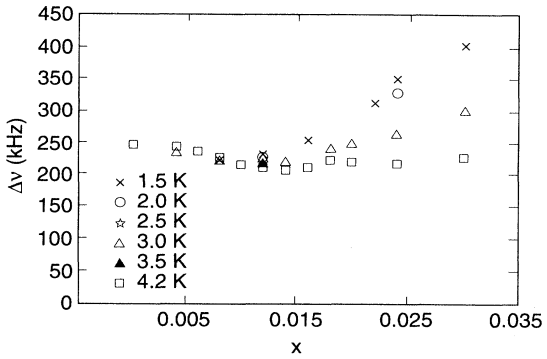

FIG. 13. Zeeman splitting $\Delta\nu$ of the $2\nu_Q$ ^{139}La NQR line in $La_{2-x}Sr_xCuO_4$ as a function of Sr concentration x at several temperatures $T \leq 4.2$ K.

We now describe a simple model for the staggered magnetization for $T < 30$ K in terms of a localization transition. Note that since the magnitude of the local field at the muon site, B_μ does not depend upon the orientation of the EFG [contrary to the Zeeman splitting in Eq. (1)], one can safely rule out that the anomalies in Figs. 7(a) and 9(b) in the sublattice magnetization below 30 K are due to a long-range structural distortion and/or tilting of the CuO_6 octahedra; rather, they must arise from $M^{\dagger}(x,T)$. A plausible explanation is that below 30 K the microsegregated mobile holes get localized around the Sr substitutional atoms, such as has been proposed in Refs. 1, 4, and 21. Partial support for this conjecture follows from the success of the theory of Ref. 3 in explaining the transverse-spin freezing,[1] coupled with the μSR results.[7]

To be specific, the theory accurately predicts the doping dependence of the spin-freezing temperature T_f but is based on the assumption that this is not a true phase transition, instead being a continuous freezing of the transverse-spin distortions generated by localized carriers. Measurements of the longitudinal decay rate λ of the muon polarization [see Eq. (5)] performed on a sample with $x = 0.008$ do indeed support the notion of a continuous freezing of the transverse-spin components. The data, shown in Fig. 14, exhibit a broad maximum in λ which shifts slightly and is largely suppressed by the application of an external magnetic field H. A simple model of the muon longitudinal relaxation due to a continuous slowing down of the transverse Cu^{2+} spin components predicts, in analogy with the fluctuations of NMR-NQR nuclear-spin-lattice relaxation rate,[1] that the maximum of λ should occur when $\omega\tau \approx 1$, where $\omega = \gamma_\mu H$ is the muon precession frequency and τ is an average effective correlation time of the transverse-spin fluctuations. Furthermore, the maximum value of λ should scale approximately as $\lambda \propto 1/\omega$ (for $H = 0$ the precession frequency $\omega = \gamma_\mu B_\mu \approx 5.7$ MHz corresponds to the local internal field $B_\mu \approx 420$ G [see Fig. (9b)]. When an external magnetic field is applied, the local field at the muon site ac-

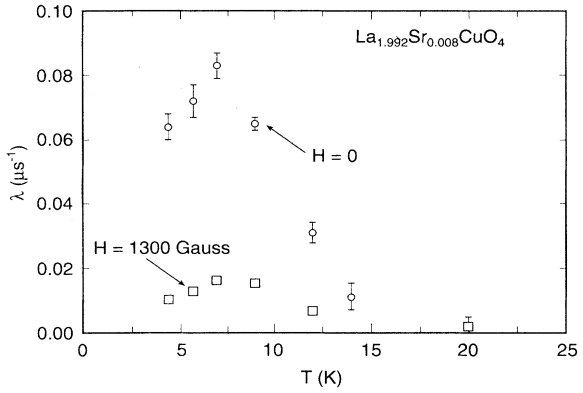

FIG. 14. Longitudinal decay rate λ of the muon polarization signal in $La_{2-x}Sr_xCuO_4$ ($x=0.008$), plotted vs temperature T for: (○) zero applied field; (□) applied field of 1300 G.

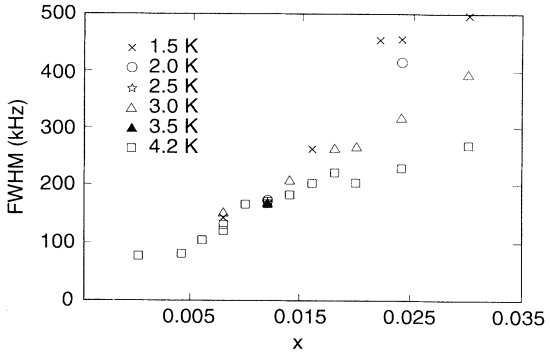

FIG. 15. Full width at half maximum intensity (FWHM) of the $2\nu_Q$ ^{139}La NQR line in $La_{2-x}Sr_xCuO_4$ as a function of Sr concentration x at several temperatures $T \leq 4.2$ K.

quires a wide intensity distribution due to the different mutual orientations of $\mathbf{H}$ and $\mathbf{B}_\mu$ with average value approximately equal to the external field, yielding $\omega=\gamma_\mu H \approx 17.5$ MHz. The depression of the maximum in λ with increasing ω is qualitatively in agreement with the data in Fig. 14. On the other hand, the predicted frequency shift of the maximum cannot be established firmly due to the broad distribution of internal fields which broaden the maximum of λ. The position of the maximum of λ, which defines the freezing temperature T_f is generally consistent with the maximum of the NQR relaxation rate R_1 in Ref. 1 considering that the resonance frequencies are not much different in the different sets of experiments.

Further support for this localization follows from the notion that a local distortion of the EFG and of the internal field around the localized holes is expected to give rise to broadening effects in the NQR line proportional to the doping concentration x as is normally observed in crystals containing dilute paramagnetic impurities and/or lattice defects. This is indeed what is observed, as is shown in Fig. 15, where the linewidth shows a linear dependence on x. As explained above, here one should only consider the data for $x<0.02$ for which the system is in a state with long-range AF order.

This localization of the holes at very low temperatures is consistent with measurements of ac and dc resistivity in the same system.[22] Also, spin-freezing effects similar to the ones observed in $La_{2-x}Sr_xCuO_4$ (Fig. 14 and Ref. 1) below the localization temperature, have been observed also in $La_2Cu_{1-x}Zn_xO_4$ where they have been ascribed to the freezing of the extra local moment induced in the CuO_2 plane by Zn doping.[20]

A problem which remains largely unsolved concerns the location and the electronic structure in the La_2CuO_4 lattice of the localized hole at $T=0$. The spin texture generated by a hole localized on a plaquette of four Cu spins in the CuO_2 plane according to the model in Refs. 3 and 4 or from an oxygen hole localized on a single Cu-O bond,[23] predicts[18] a reduction of the sublattice magnetization $M^\dagger(0,x)$ upon increasing concentration larger than the one shown by the data in Figs. 10 and 12. One could speculate that at the lowest temperatures the holes move close to the apical oxygen sites thus removing any effect on the Cu spins in the plane. Further experiments that could scrutinize the idea that the localization at such low temperatures leads to holes in the apical oxygen sites could possible involve extended x-ray-absorption fine structure and/or ^{17}O NMR experiments in single crystals.

VIII. SUMMARY AND CONCLUSIONS

We have used ^{139}La nuclear quadrupole resonance (NQR) and positive muon spin rotation (μSR) measurements to probe the weakly doped antiferromagnetic (AF) region ($x<0.02$) of the $La_{2-x}Sr_xCuO_4$ system below the three-dimensional (3D) AF ordering (Néel) temperature $T_N(x)$. The temperature dependence of the *local magnetic field magnitude at the muon site* $B_\mu(x,T)$, determined from the μSR measurements, is found to be in essential agreement with that of the *component* $H^{\parallel}_{\rm int}(x,T)$ *of the local field at the La site* parallel to the electric-field gradient principal axis (z' axis), determined previously from the Zeeman splitting of the $2\nu_Q$ ^{139}La NQR transition for the same samples,[1] augmented by the present NQR measurements for $x=0.018$. This agreement shows that both $B_\mu(x,T)$ and $H^{\parallel}_{\rm int}(x,T)$ are measures of the Cu^{2+} staggered magnetization $M^\dagger(x,T)$ below $T_N(x)$. From auxiliary ^{139}La nuclear magnetic resonance (NMR) measurements of a single crystal of $La_2CuO_{4+\delta}$ with $T_N=308$ K, the quantitative differences found between the temperature dependences of $B_\mu(x,T)$ and $H^{\parallel}_{\rm int}(x,T)$ are due to the fact that the component $H^{\parallel}_{\rm int}(x,T)$ is not strictly proportional to the magnitude $H_{\rm int}$. This effect is ascribed mainly to the temperature-dependent orientation of the z' axis with respect to the crystal c axis, with a small contribution coming from the temperature dependence of the orientation of $\mathbf{H}_{\rm int}$ with respect to the c axis and/or of the mutual orientation of the projections of $\mathbf{H}_{\rm int}$ and z' axis onto the ab plane.

Above ~ 30 K, $M^{\dagger}(x,T)$ at each T is found to be progressively depressed with increasing x (decreasing T_N). The $M^{\dagger}(x,T=0)$ values, *extrapolated from* $T > 30$ K, are found from both the μSR and NQR measurements to follow the same empirical relation $M^{\dagger}(x,0)/M^{\dagger}(0,0) = (1-x/x_c)^n$ with $x_c = 0.023$ and $n = 0.236$. To model $M^{\dagger}(x,0)$, we assume that the doped holes are mobile and are situated in 1D "rivers" of charge which form walls in the CuO_2 planes separating undoped AF domains; an infinite number of these layers are stacked along the c axis. Using linear spin-wave theory, we calculated $M^{\dagger}(x,0)$ for this hole and spin configuration and found good agreement with the experimental extrapolated values using the Cu^{2+} intraplanar and interplanar AF exchange interactions from neutron-scattering results reported[5] for La_2CuO_4. Thus, *in the AF region* $x < 0.02$ of the phase diagram of $La_{2-x}Sr_xCuO_4$, our results support the previous hypothesis[1,2,8] that microsegregation of the (mobile) doped holes into domain walls occurs, consistent with the phase separation phenomenology of Emery and Kivelson.[10]

Below ~ 30 K, an anomalous increase in $M^{\dagger}(x,T)$ occurs in $La_{2-x}Sr_xCuO_4$ such that the observed staggered magnetization is nearly independent of x as $T \rightarrow 0$ and is about the same as the corresponding value for undoped La_2CuO_4. As in our previous work,[1,7] we interpret this effect as arising from doped-hole localization occurring below ~ 30 K. In support of this hypothesis, we find that the width of the ^{139}La NQR $2\nu_Q$ line is nearly independent of temperature below 4.2 K and increases linearly with x. As reported before,[1] the spin degrees of freedom associated with the doped holes undergo, below the localization temperature, a spin-freezing at $T_f = (815$ K$)\,x$ superimposed on the long-range AF background. The field-dependent μSR data presented here support the idea that a continuous spin freezing occurs rather than a true phase transition.

ACKNOWLEDGMENTS

Thanks are due to A. Rigamonti for stimulating discussions. Ames Laboratory is operated for the U.S. Department of Energy by Iowa State University under Contract No. W-7405-Eng-82. The work at Ames was supported by the Director for Energy Research, Office of Basic Energy Sciences. The work at Pavia was supported by Instituto Nazionale Fisica della Materia. One of us (R.J.G.) acknowledges support by NSERC of Canada.

*Present address: Superconductivity Technology Center, Mail Stop K763, Los Alamos National Laboratory, Los Alamos, NM 87545.

†Present address: Center for Materials Science and Engineering, Massachusetts Institute of Technology, Cambridge, MA 02139.

[1] F. C. Chou, F. Borsa, J. H. Cho, D. C. Johnston, A. Lascialfari, D. R. Torgeson, and J. Ziolo, Phys. Rev. Lett. **71**, 2323 (1993).

[2] J. H. Cho, F. C. Chou, and D. C. Johnston, Phys. Rev. Lett. **70**, 222 (1993).

[3] R. J. Gooding, N. M. Salem, and A. Mailhot, Phys. Rev. B **49**, 6067 (1994).

[4] R. J. Gooding, Phys. Rev. Lett. **66**, 2266 (1991).

[5] B. Keimer, N. Belk, R. J. Birgeneau, A. Cassanho, C. Y. Chen, M. Greven, M. A. Kastner, A. Aharony, Y. Endoh, R. W. Erwin, and G. Shirane, Phys. Rev. B **46**, 14 034 (1992).

[6] I. Ya. Korenblit and A. Aharony, Phys. Rev. B **49**, 13 291 (1994).

[7] F. Borsa, P. Carretta, A. Lascialfari, D. R. Torgeson, F. C. Chou, and D. C. Johnston, Physica C **235-240**, 1713 (1994).

[8] J. H Cho, F. Borsa, D. C. Johnston, and D. R. Torgeson, Phys. Rev. B **46**, 3179 (1992).

[9] P. W. Anderson, Phys. Rev. **86**, 694 (1952).

[10] V. J. Emery and S. A. Kivelson, Physica C **209**, 597 (1993); see also **235-240**, 189 (1994).

[11] K. Sun, J. H. Cho, F. C. Chou, W. C. Lee, L. L. Miller, D. C. Johnston, Y. Hidaka, and T. Murakami, Phys. Rev. B **43**, 239 (1991), and references cited.

[12] H. Lütgemeier and M. W. Pieper, Solid State Commun. **64**, 267 (1987).

[13] H. Nishihara, H. Yasuoka, T. Shimizu, T. Tsuda, T. Imai, S. Sasaki, S. Kanbe, K. Kishio, K. Kitazawa, and K. Fueki, J. Phys. Soc. Jpn. **56**, 4559 (1987).

[14] D. E. MacLaughlin, J. P. Vithayathil, H. B. Brom, J. C. J. M. de Rooy, P. C. Hammel, P. C. Canfield, A. P. Reyes, Z. Fisk, J. D. Thompson, and S.-W. Cheong, Phys. Rev. Lett. **72**, 760 (1994).

[15] P. C. Hammel, A. P. Reyes, S.-W. Cheong, Z. Fisk, and J. E. Schirber, Phys. Rev. Lett. **71**, 440 (1993).

[16] A. Schenck, *Muon Spin Rotation: Principles and Applications in Solid State Physics* (Hilger, Bristol, 1986).

[17] The calculations presented here are carried out using periodic boundary conditions in the x direction. We have also completed the analogous calculation for open boundary conditions, and the results are similar. The somewhat complicated details of this calculation will be presented elsewhere (Ref. 18).

[18] K. J. E. Vos, N. M. Salem, and R. J. Gooding (unpublished).

[19] B. L. Shraiman and E. D. Siggia, Phys. Rev. Lett. **61**, 467 (1988).

[20] M. Corti, A. Lascialfari, A. Rigamonti, F. Tabak, F. Licci, and L. Raffa, J. Appl. Phys. **75**, 7143 (1994); (unpublished).

[21] K. M. Rabe and R. N. Bhatt, J. Appl. Phys. **69**, 4508 (1991).

[22] C. Y. Chen, R. J. Birgeneau, M. A. Kastner, N. W. Preyer, and T. Thio, Phys. Rev. B **43**, 392 (1991), and references therein.

[23] A. Aharony, R. J. Birgeneau, A. Coniglio, M. A. Kastner, and H. E. Stanley, Phys. Rev. Lett. **60**, 1330 (1988).